TiO_2 Nanotubes with Tunable Morphology, Diameter, and Length: Synthesis and Photo-Electrical/Catalytic Performance

Daoai Wang,[†,‡] Ying Liu,[†,‡] Bo Yu,[†] Feng Zhou,[*,†] and Weimin Liu[†]

State Key Laboratory of Solid Lubrication, Lanzhou Institute of Chemical Physics, Chinese Academy of Sciences, Lanzhou 730000, P. R. China, and Graduate School, Chinese Academy of Sciences, Beijing 100039, P. R. China

Received September 3, 2008. Revised Manuscript Received December 12, 2008

This article reports on the synthesis of TiO_2 nanotubes (NTs) with tunable morphologies by adjusting the reaction conditions during anodization to balance electrochemical reaction and chemical etching. Nanoporous and free-standing NTs with different lengths and diameters are thus obtained in a controlled manner, solving the bundling, sealing, and etching pit issues in the conventional anodization. The high growth speed (60 μm/h) of TiO_2 NT arrays with the pore diameter of 120 nm was achieved. The photoelectrochemical response of the NT photoelectrodes is studied under both UV and visible illumination from 250 to 600 nm, showing that the photoresponse occurred between 300−400 nm with the maximum value at 355 nm. The nanoporous TiO_2 film has the higher photocurrent density than the nonporous NTs array because of fewer defects and perfect alignment. However, the photocatalytic performance to degrade methylene blue showed an inverse trend: the free-standing TiO_2 NTs have better photocatalytic degradation than the nanoporous TiO_2 NT film probably due to the larger effective contact area.

1. Introduction

Nanostructured materials, especially the ordered nanotube materials, have attracted a great deal of attention in various fields due to their numerous technological applications.[1] Recently, electrochemically anodized TiO_2 nanotube arrays have demonstrated their prospective applications in making dye-sensitized solar cells,[2] as electrochemical sensors,[3] as the photocatalysts,[4] as the template to make one-dimensional materials,[5] as water-splitting catalysts for hydrogen generation,[6] and so forth. In all of these applications, the structures of TiO_2 NTs including the diameter, the length of tubes, and the structure of the top surface of the NTs, have profound effects on their performance.

TiO_2 NT arrays with large surface area, that are defect free, and have perfect alignment have been the pursuit of a large amount of studies. The synthesis of TiO_2 NT arrays was initialized by Gong and co-workers using aqueous HF solution.[7−9] However, only 500 nm length NTs were obtained, and it was very difficult to get the self-supporting TiO_2 NTs.[7] Later on, anodization in nonaqueous polar solvents was introduced to get the TiO_2 NT array with high aspect ratios, such as glycerol, dimethyl sulfoxide (DMSO), formamide (FA), ethylene glycol, and *N*-methylformamide (NMF) with[10,11] or without fluoride ions,[12] opening new pages for TiO_2 NT production. A new benchmark was created by Grimes et al.,[13] in whose work the NTs with the aspect ratio larger than 2200 and the length over 1 mm were achieved. Unfortunately, most of those products have the bundling

* To whom correspondence should be addressed. E-mail: zhouf@lzb.ac.cn.
† Lanzhou Institute of Chemical Physics.
‡ Chinese Academy of Sciences.

(1) Xia, Y.; Yang, P. D.; Sun, Y.; Wu, Y.; Mayers, B.; Gates, B.; Yin, Y.; Kim, F.; Yan, H. *Adv. Mater.* **2003**, *15*, 353. Hueso, L.; Mathur, N. *Nature* **2004**, *427*, 301. Grimes, C. A. *J. Mater. Chem.* **2007**, *17*, 1451. Mwaura, J. K.; Zhao, X.; Jiang, H.; Schanze, K. S.; Reynolds, J. R. *Chem. Mater.* **2007**, *19*, 1202.
(2) Mor, G. K.; Shankar, K.; Paulose, M.; Varghese, O. K.; Grimes, C. A. *Nano Lett.* **2006**, *6*, 215. Shankar, K.; Mor, G. K.; Prakasam, H. E.; Varghese, O. K.; Grimes, C. A. *Langmuir* **2007**, *23*, 12445. Kuang, D.; Brillet, J.; Chen, P.; Takata, M.; Uchida, S.; Miura, H.; Sumioka, K.; Zakeeruddin, S. M.; Grätzel, M. *ACS Nano* **2008**, *2*, 1113.
(3) Zheng, Q.; Zhou, B.; Bai, J.; Li, L.; Jin, Z.; Zhang, Z.; Li., J.; Liu, Y.; Cai, W.; Zhu, X. *Adv. Mater.* **2008**, *20*, 1044. Liu, S.; Chen, A. *Langmuir* **2005**, *21*, 8409. Mor, G. K.; Varghese, O. K.; Paulose, M.; Ong, K. G.; Grimes, C. A. *Thin Solid Films* **2006**, *496*, 42.
(4) Albu, S. P.; Ghicov, A.; Macak, J. M.; Hahn, R.; Schmuki, P. *Nano Lett.* **2007**, *7*, 1286. Zhang, Z.; Yuan, Y.; Shi, G.; Fang, Y.; Liang, L.; Ding, H.; Jin, L. *Environ. Sci. Technol.* **2007**, *41*, 6259.
(5) Macak, M. J.; Gong, G. B.; Hueppe, M.; Schmuki, P. *Adv. Mater.* **2007**, *19*, 3027. Yang, L.; He, D.; Grimes, C. A.; Cai, Q. *J. Phys. Chem. C* **2007**, *111*, 8214. Yang, L.; Yang, W.; Cai, Q. *J. Phys. Chem. C* **2007**, *111*, 16613.
(6) Park, J. H.; Kim, S.; Bard, A. J. *Nano Lett.* **2006**, *6*, 24.
(7) Gong, D.; Grimes, C. A.; Varghese, O. K.; Hu, W. C.; Singh, R. S.; Chen, Z.; Dickey, E. C. *J. Mater. Res.* **2001**, *16*, 3331.
(8) Ghicov, A.; Tsuchiya, H.; Macak, J. M.; Schmuki, P. *Phys. Status Solidi* **2006**, *203*, 28. Ghicov, A.; Tsuchiya, H.; Hahn, R.; Macak, J. M.; Mu, A. G.; Schmuki, P. *Electrochem. Commun.* **2006**, *8*, 528. (b) Funk, S.; Hokkanen, B.; Burghaus, U.; Ghicov, A.; Schmuki, P. *Nano Lett.* **2007**, *7*, 1091.
(9) Xie, Y. *Adv. Funct. Mater.* **2006**, *16*, 1823.
(10) Ruan, C.; Paulose, M.; Varghese, O. K.; Mor, G. K.; Grimes, C. A. *J. Phys. Chem. B* **2005**, *109*, 15754. Paulose, M.; Shankar, K.; Yoriya, S.; Prakasam, H. E.; Varghese, O. K.; Mor, G. K.; Latempa, T. A.; Fitzgerald, A.; Grimes, C. A. *J. Phys. Chem. B* **2006**, *110*, 16179. Yoriya, S.; Paulose, M.; Varghese, O. K.; Mor, G. K.; Grimes, C. A. *J. Phys. Chem. C* **2007**, *111*, 13770. Yoriya, S.; Prakasam, H. E.; Varghese, O. K.; Shankar, K.; Paulose, M.; Mor, G. K.; Latempa, T. J.; Grimes, C. A. *Sens. Lett.* **2006**, *4*, 334. Shankar, K.; Mor, G. K.; Fitzgerald, A.; Grimes, C. A. *J. Phys. Chem. C* **2007**, *111*, 21–26.
(11) Macak, J. M.; Tsuchiya, H.; Taveira, L.; Aldabergerova, S.; Schmuki, P. *Angew. Chem., Int. Ed.* **2005**, *44*, 7463.
(12) Allam, N. K.; Grimes, C. A. *J. Phys. Chem. C* **2007**, *111*, 13028. Chen, X.; Schriver, M.; Suen, T.; Mao, S. S. *Thin Solid Films* **2007**, *515*, 8511.
(13) Prakasam, H. E.; Shankar, K.; Paulose, M.; Varghese, O. K.; Grimes, C. A. *J. Phys. Chem. C* **2007**, *111*, 7235.

10.1021/cm802384y CCC: $40.75
Published on Web 03/05/2009

problem on the top layer of NTs, which is mainly induced by the capillary force, the overetching of the top parts, and the high aspect ratio. The bundling does not only affect the exciton transport and recombination dynamics in TiO_2 NT based solar cells[14] and also have an impact on the infiltration of interacted materials. Although the post-treatments of supercritical, HF etching, and mild ultrasonication methods can significantly improve the alignment,[15−17] the issue is far from being solved. On the other hand, people may get bundling-free TiO_2 NTs, but the sealing and etching pits on the surface will probably deteriorate the performance and restrict their applications.[18] People have to compromise between bundling, high aspect ratio and top surface morphology of the TiO_2 NT arrays. To solve all of these problems we introduced a simple protocol to prepare perfectly aligned and high aspect ratio nanoporous NTs in ethylene glycol containing mixture electrolytes of HF and NH_4F. According to detailed investigation, it is found that anodization conditions have profound effects on the surface morphologies, such as the temperature, anodic voltage, anodization time, HF concentration, and so forth, intrinsically by altering the comparative electrochemical anodization speed and chemical etching speed. As a consequence, in nanoporous or free-standing TiO_2 NTs with the controllable pore size from 20 nm to 160 nm, the length from several hundred nanometers to several hundred micrometers can be easily synthesized. The photoelectrochemical response[19] of the TiO_2 NTs was studied under the concolorous illumination from 250 to 600 nm. The photocatalytic performance[3,20] of these materials to degrade methylene blue was also compared under the UV illumination of 355 nm.

2. Experimental Section

Highly oriented TiO_2 nanotube and nanopore arrays were prepared by a potentiostatic anodization in a two-electrode electrochemical cell. The commercial titanium foil (250 μm thick, Alfa Aesar, purity 99.5%) was used as a working electrode, and a graphite slice served as a counter electrode. The titanium foils were washed with ethanol and acetone for about 20 min by ultrasonication to remove the contamination, then completely washed with distilled water, and finally dried in the air prior to anodization. These foils were anodized at different direct current (DC) voltages applied by a DC power supply (LW10J2, Shanghai) in an electrolyte solution containing ethylene glycol, hydrofluoric acid, and 0.5 wt % NH_4F.

Scheme 1. Schematic of Fabricating Controllable TiO_2 NT Array via Adjusting the Reaction Conditions[a]

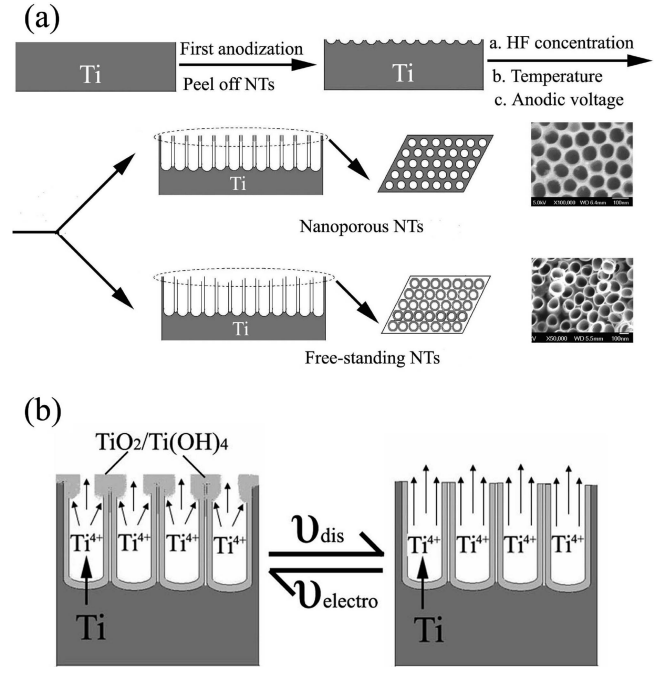

[a] $\upsilon_{electro}$: anodization speed. υ_{dis}: chemical etching speed.

The anodization voltages were varied from 10 to 200 V; HF concentration varied from 0.1 to 10 vol %, and the temperature varied from −5 to 60 °C. To decrease the defect on the surface, the samples were pre-anodized[21] in a 0.5 wt % NH_4F ethylene glycol solution at 60 V for 2 h, and then the NT film was removed by ultrasonication in 1 M HCl aqueous solution. After anodization, the samples were washed with deionized water and then dried in air. To measure the photocurrent and photocatalytic properties, the as-prepared amorphous TiO_2 NTs were annealed at 500 °C for 2 h to get the anatase TiO_2 NT arrays without distinguishable morphology changes (the length and pore size). The morphology of the TiO_2 NT array was investigated by use of a field emission scanning electron microscope (JSM-6701F, JEOL Inc., Japan). The photoelectrochemical response of the TiO_2 NT photoelectrodes was studied at the excitation wavelength between 250 and 600 nm using a 150 W xenon lamp of SM-25 Hyper Monolight (Japan) system with a CHI660B electrochemical workstation. The photocatalytic activity of the prepared TiO_2 NT array was evaluated under the excitation wavelength of 355 nm. The pulse train was guided into a quartz cuvette filled with a 2 mL aqueous solution of methylene blue (1×10^{-5} M) and a TiO_2 NT sheet with the area of 1 cm^2. The decomposition of the solute was followed by measuring the absorption of the methylene blue in solution with a UV−vis spectrometer. The sample was first kept in the dark for 6 h to completely adsorb dissolved methylene blue. Then the filled cuvette was exposed to the irradiation of the 355 nm laser pulse.

3. Results and Discussion

3.1. Mechanisms of Anodization. The synthetic process of the TiO_2 NT array is shown in Scheme 1a. Two-step anodization was adopted to better control the surface morphology. In the first anodization step, the NTs with

(14) Williams, S. S.; Hampton, M. J.; Gowrishankar, V.; Ding, I. K.; Templeton, J. L.; Samulski, E. T.; DeSimone, J. M.; McGehee, M. D. *Chem. Mater.* **2008**, *20*, 5229. Goh, C.; Coakley, K. M.; McGehee, M. D. *Nano Lett.* **2005**, *5*, 1545. Coakley, K. M.; McGehee, M. D. *Appl. Phys. Lett.* **2003**, *83*, 3380. Zhu, K.; Neale, N. R.; Miedaner, A.; Frank, A. J. *Nano Lett.* **2007**, *7*, 69.
(15) Paulose, M.; Prakasam, H. E.; Varghese, O. K.; Peng, L.; Popat, K. C.; Mor, G. K.; Desai, T. A.; Grimes, C. A. *J. Phys. Chem. C* **2007**, *111*, 14992.
(16) Zhu, K.; Vinzant, T. B.; Neale, N. R.; Frank, A. J. *Nano Lett.* **2007**, *7*, 3739.
(17) Wang, J.; Lin, Z. *Chem. Mater.* **2008**, *20*, 1257.
(18) Mor, G. K.; Varghese, O. K.; Paulose, M.; Shankar, K.; Grimes, C. A. *Sol. Energy Mater. Sol. Cells* **2006**, *90*, 2011.
(20) Gole, J. L.; Stout, J. D.; Burda, C.; Lou, Y.; Chen, X. *J. Phys. Chem. B* **2004**, *108*, 1230. Miyauchi, M.; Nakajima, A.; Fujishima, A.; Hashimoto, K.; Watanabe, T. *Chem. Mater.* **2000**, *12*, 3.
(19) Hahn, R.; Stergiopoulus, T.; Macak, J. M.; Tsoukleris, D.; Kontos, A. G.; Albu, S. P.; Kim, D.; Ghicov, A.; Kunze, J.; Falaras, P.; Schmuki, P. *Phys. Status Solidi* **2007**, *1*, 135. Kim, D.; Macak, J. M.; Schimidt-Stein, F.; Schmuki, P. *Nanotechnology* **2008**, *19*, 305710.
(21) Macak, J. M.; Albu, S. P.; Schmuki, P. *Phys. Status Solidi (RRL)* **2007**, *1*, 181. Zhang, G.; Huang, H.; Zhang, Y.; Chan, H. L. W.; Zhou, L. *Electrochem. Commun.* **2007**, *9*, 2854.

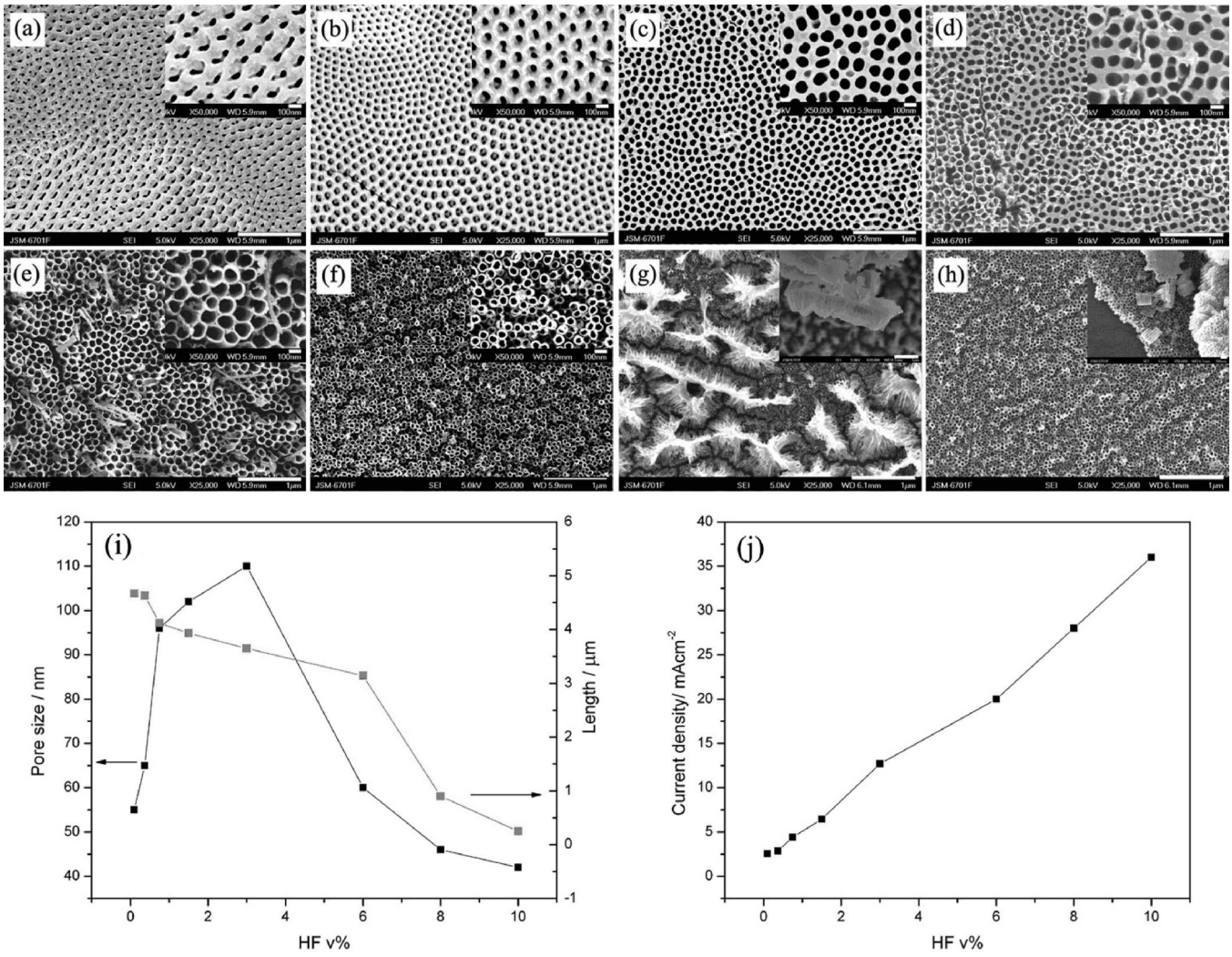

Figure 1. The effect of HF concentration on the surface morphologies of TiO_2 NTs. The samples were anodized at 60 V for 1 h at 15 °C in a mixture NH_4F and HF with different HF concentrations of (a) 0.1 vol %, (b) 0.37 vol %, (c) 0.75 vol %, (d) 1.5 vol %, (e) 3 vol %, (f) 6 vol %, (g) 8 vol %, and (h) 10 vol %. (i) The evolution of pore size and the length of NTs with HF concentration. (j) Variation of stable anodic current density with HF concentration.

random morphologies were obtained and peeled off by ultrasonic in 1 M HCl aqueous solution, leaving ordered bowl-like footprints on the titanium substrate. The second step of the anodization process was carried out in a mixture of HF and NH_4F ethylene glycol solution. Scheme 1b shows two competitive reactions during the formation of TiO_2 NTs.[10,18,22] At the anode, metal Ti is dissolved concurrent with the electrolysis of water and the release of O_2 and local pH decrease corresponding to the electrochemical anodization ($v_{electro}$). Ti is dissolved and ejected from nanopore to outside and accumulated at the entrance of nanopores, where TiO_2 precipitate [most possibly the $Ti(OH)_4$] is formed via the instantaneous hydrolysis reaction. This leads to the generation and the accumulation of $Ti(OH)_4$ precipitate at the entrance of nanopores. At the same time, the dissolution of TiO_2 in the presence of fluoride and high acidic environment also occurs corresponding to the chemical etching (v_{dis}), and hydrogen fluoride is consumed, which is the key in controlling the surface morphology. Any reaction conditions affecting the reaction equilibrium will alter the surface morphology. These factors may include the concentration of the electrolyte, the reaction temperature, the anodization voltage, the reaction time, and so on. So, we can adjust the balance to control the morphology of TiO_2 NTs by changing the reaction conditions. For instance, if the v_{dis} is smaller than the $v_{electro}$, the nanoporous TiO_2 NTs will be formed. Otherwise, the nonporous TiO_2 NT array will be favored. The comparative values of $v_{electro}$ and v_{dis} will also determine the growth speed of NTs.

3.2. Effect of HF Concentration. Hydrogen fluoride plays a key role in controlling the surface morphology. HF acts as pore opening reagent. Without HF, the top surfaces of NT arrays are usually covered by the TiO_2 precipitate which may block further anodization after a certain amount of accumulation. If the concentration of HF is too high, the top deposits will be easily dissolved, leaving an overetching orifice. However, excess HF may deteriorate the intact structure of NTs, resulting in a large number of defects. Figure 1 shows the FESEM images of the top surface morphologies of the prepared TiO_2 NTs obtained with various HF concentrations from 0.1 vol % to 10 vol %. It is clearly seen that at low HF concentra-

(22) Kang, S. H.; Kim, J.; Kim, H. S.; Sung, Y. *J. Ind. Eng. Chem.* **2008**, *14*, 52.

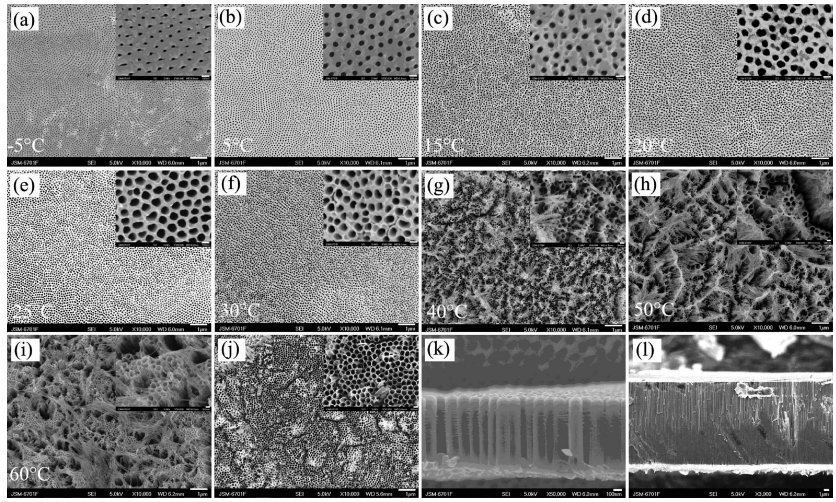

Figure 2. FESEM images of TiO_2 NTs arrays grown from a 0.5 wt % NH_4F and 1 vol % HF ethylene glycol electrolyte for 1 h at 60 V with various anodization temperature from −5 (a) to 60 °C (i), respectively. (j) The FESEM image of (h) after ultrasonication. Cross sectional images of (a) and (i) are seen in (k) and (l).

tions (Figure 1a,b) the size of the pores was very small, and the shapes were not very regular on the top, which resulted from rapid ejection of TiO_2 precipitate. With the increase of the HF concentration, the size of the pores turned bigger, and the shape also became more regular (Figure 1c). When further increased to 1.5 vol %, some parts of the nanoporous structure started to be damaged, indicating the v_{dis} exceeded $v_{electro}$. Free standing NTs started to form on the top surface. When the concentrations were above 3 vol %, the nanoporous structure disappeared. Further increasing the concentration of HF, the pore size decreased, and there appeared some bundling NTs on the top surface when the concentration of HF was 8 vol %. When the content of HF reached 10 vol %, the bundling structure disappeared, leaving the overetching TiO_2 NTs with very short length. The relationships among the HF concentration, pore size, and length of the NTs are presented in Figure 1i, and the relationship between the HF concentration and the stable current density is shown in Figure 1j. It is seen that the length decreased progressively with increasing HF concentration because of the speedup of chemical etching. The pore size increased with the addition of HF from 0.1 vol % to 3 vol %, from 55 to 108 nm, as a result of removal of overwhelmed TiO_2 precipitate and lateral etching of newly formed nanotubes having very thick walls. Further increasing the concentration of HF, the length of the NTs further decreased even to 250 nm (10 vol % HF) due to the rapid etching of NTs both in the vertical direction and in the lateral direction (the decrease of the thickness of the wall). At the same time the pore size also decreased because of the high HF concentration and the repaid chemical etching speed. From these results we can see that the morphologies, the sizes, and the shapes of NTs of the as-prepared TiO_2 NT arrays were strongly affected by the concentration of HF. The top surface morphology can be tuned from nanoporous to open nanotube structures.

3.3. Effect of Temperature. Figure 2 shows the top surface FESEM images of samples prepared in the 0.5 wt % NH_4F and 1 vol % HF ethylene glycol electrolyte solution anodized at 60 V for 1 h with various anodization temperatures from −5 (a) to 60 °C (i). The relationships between the pore size and the length of NTs and the reaction temperatures are shown in Figure 3a, and the relationship between the reaction temperature and the current density is shown in Figure 3b. From these images and data we can see that at low temperature (−5 °C) both v_{dis} and $v_{electro}$ were very low. The low $v_{electro}$ can be seen from the low current density and the small NT length of about 0.92 μm (Figure 2k). The irregular pore shapes and small sizes (Figure 2a) indicated low v_{dis} so that TiO_2 precipitate accumulated on the top surface cannot be removed rapidly even though the $v_{electro}$ was small. The nanoporous TiO_2 NTs with high quality can be obtained at 5 °C with the very regular pores without defect at large area (Figure 2b and the inset). At this condition, the v_{dis} and $v_{electro}$ had a good balance, although the NT growth speed was not very quick with the speed of about 2 μm/h. However, the pore size enlargement was significant. This may imply that temperature had a more obvious effect on the chemical etching process. With the increasing of the reaction temperature from 15 to 25 °C, porous NT arrays formed with the pore size turn bigger and bigger. Upon further increase of the temperature to 35 °C, part of the nanoporous structure started to be destroyed, leaving the mixtured morphology of both nanoporous and free-standing structural NTs on the top surface (Figure 2f,g). When the reaction temperature was above 40 °C, the nanoporous structure completely disappeared. The surfaces of the as-anodized nanotubes were covered with some bundling NTs and NT debris (Figure 2g−i). These bundled NTs and NT debris can be removed by simple sonication (Figure 2j). However, the underlying NTs still maintained very well orientation which can be seen by the cross sectional images in Figure 2l. The pore size and the NT length increased with the increase of the reaction temperature from −5 to 40 °C, from 37 to 138 nm, and from 0.92 to 7.28 μm. Upon further increase of temperature, the enlargement of pore size turned slow

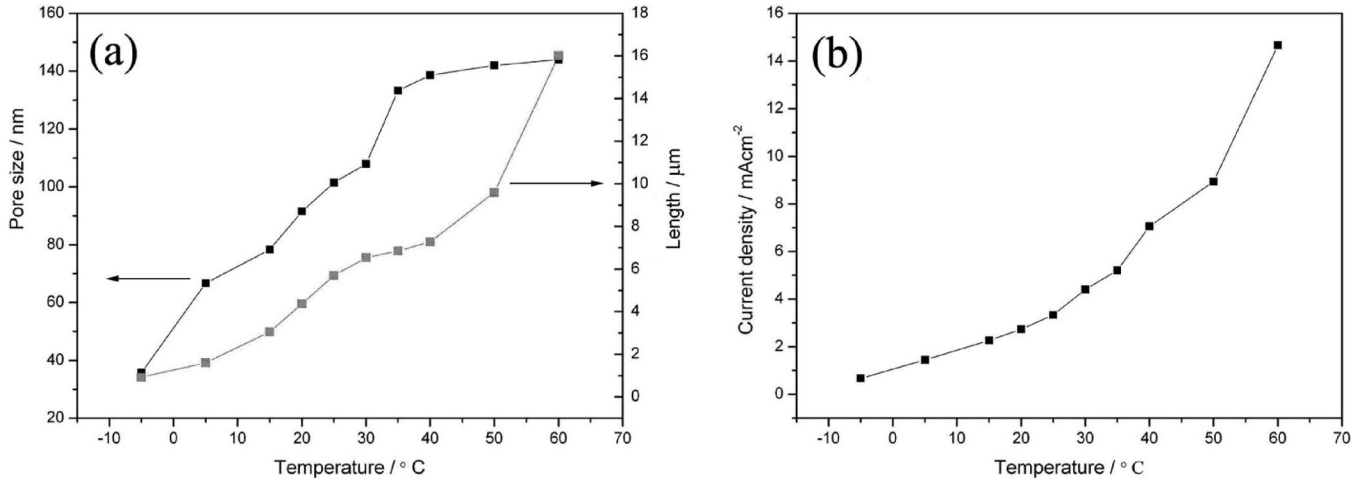

Figure 3. (a) Variation of TiO_2 nanotube array length and pore size as functions of anodization temperature at 60 V for 1 h. (b) Stable current density with different reaction temperature from −5 to 60 °C.

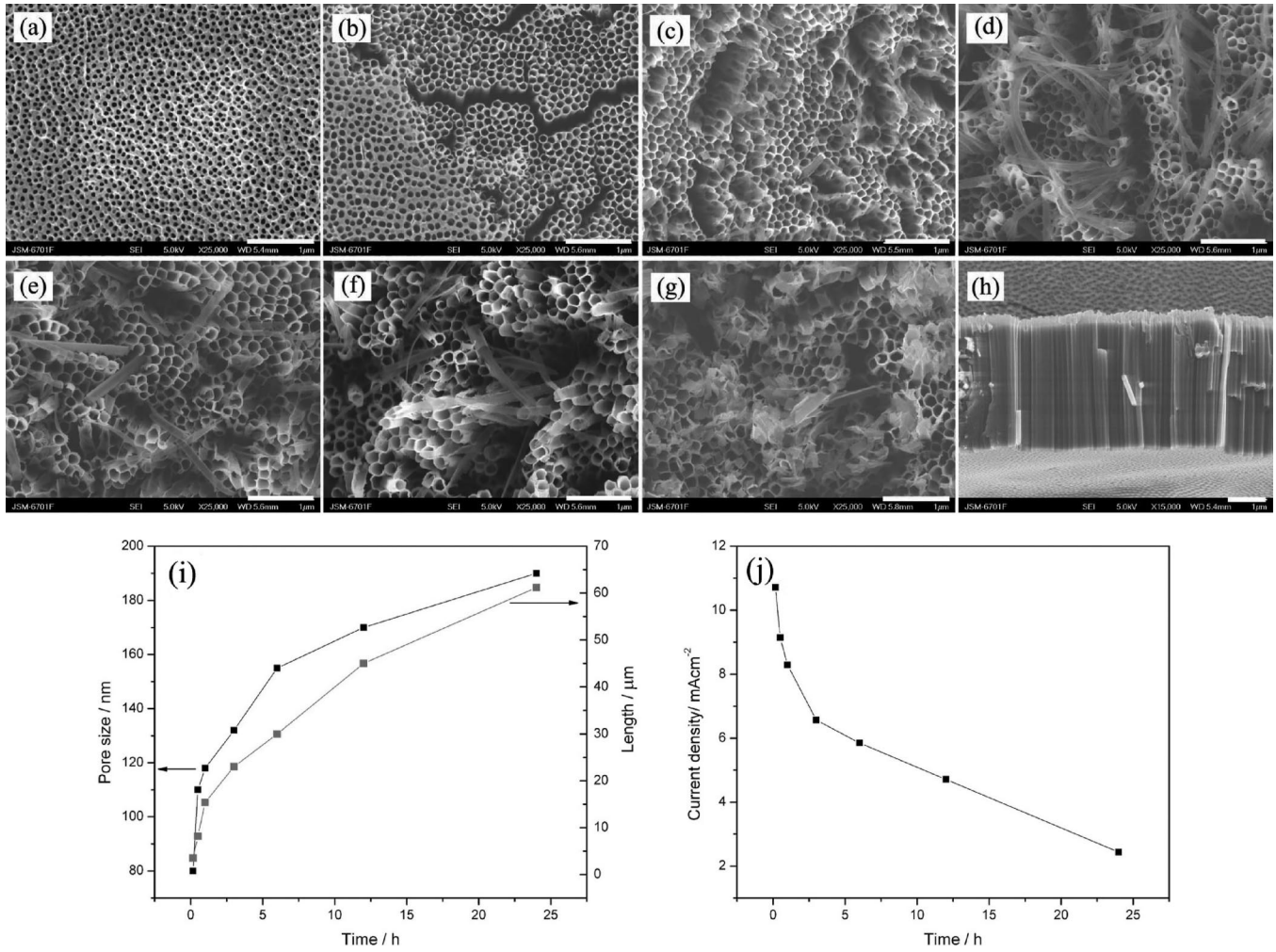

Figure 4. Effect of anodization time on the surface morphologies of TiO_2 NTs film anodized at 80 V from 10 min (a) to 24 h (h). (i) The evolution of pore size and the length of NTs with anodization time. (j) Variation of stable anodic current density with anodization time.

while the length increased quickly (Figure 3a). The chemical etching velocity also turned quicker which was far bigger than the precipitate depositing speed, while it was still much lower than the electrochemical anodization speed. So, The NTs grew very quickly with nonporous top surface. This can also be seen from the increase of the current density from 40 to 60 °C (Figure 3b). From these results we can see that the reaction temperature can affect the v_{dis} and $v_{electro}$, especially the v_{dis} at the early stage and the $v_{electro}$ at the late stage. At the late stage, consumption of HF also made the v_{dis} slower. In summary, nanoporous and nonporous NT morphology, the pore size,

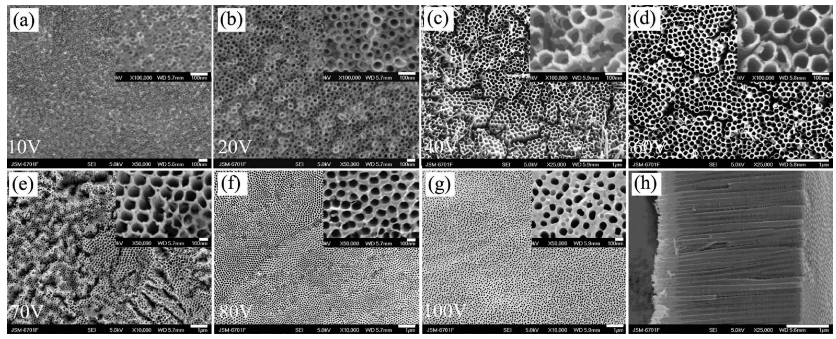

Figure 5. FESEM images of TiO_2 NT array grown from a 0.5 wt % NH_4F and 2 vol % HF ethylene glycol electrolyte for 1 h at 20 °C with various anodization voltages from 10 (a) to 100 V (g), respectively. Cross sectional image of (f) is seen in (h).

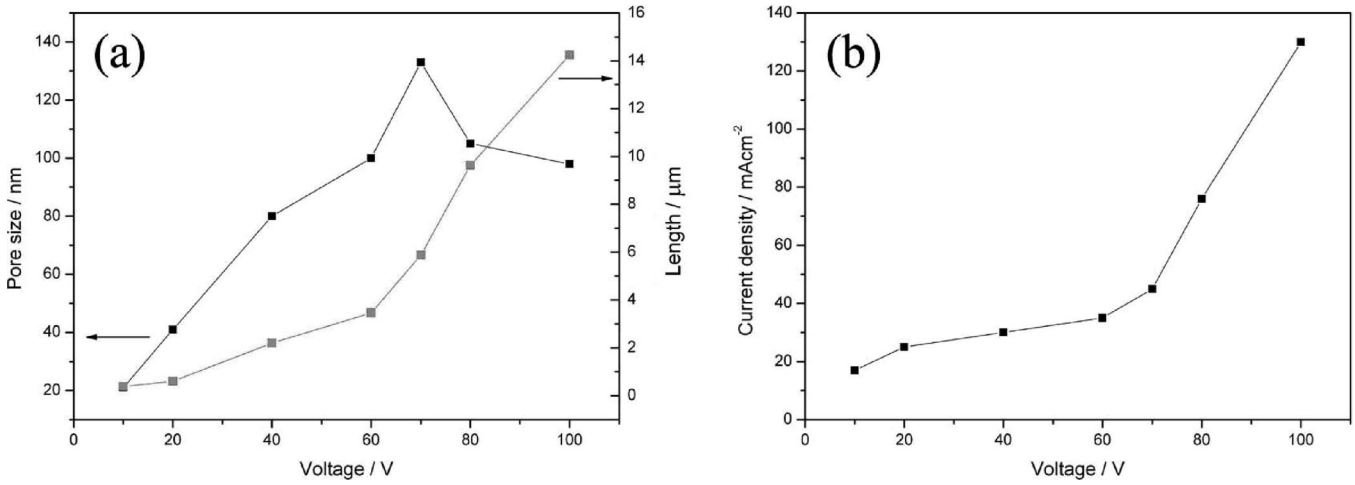

Figure 6. (a) Variation of TiO_2 NT array length and pore size as functions of anodization voltage at 20 °C for 1 h. (b) Stable current density with different anodization voltage from 10 to 100 V.

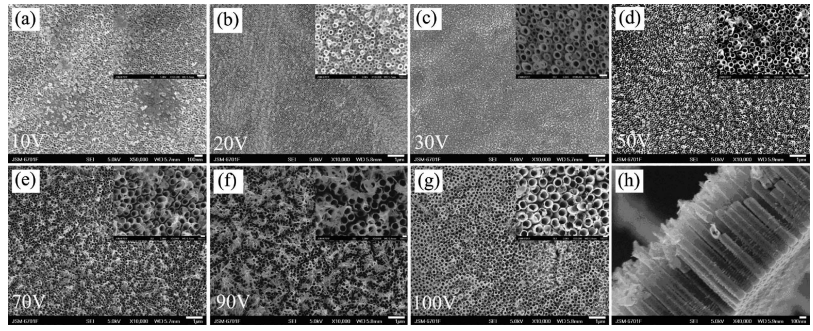

Figure 7. FESEM images of TiO_2 NTs array grown from a 0.5 wt % NH_4F and 4 vol % HF ethylene glycol electrolyte for 1 h at 20 °C with various anodization voltages from 10 (a) to 100 V (g), respectively. Cross sectional image of (d) is seen in (h).

the wall thickness, and the NT length can be controlled by the reaction temperature. TiO_2 NTs with big length can be achieved quickly at a high reaction temperature.

3.4. Time Dependence. Anodization time also plays an important role in controlling the surface morphology, pore size, and length of TiO_2 NTs. Figure 4 shows the FESEM images of the top surface morphologies of the prepared TiO_2 NTs obtained with various anodization times from 10 min to 24 h. It is seen that at different stages the morphology, the pore size, the length, and the thickness of the wall changed obviously. At the early stage, only nanoporous TiO_2 NT films were formed with small pore size (80 nm) owing to the fast $v_{electro}$ which can be seen from the big current density (Figure 4j). Then the nanoporous layer was partly dissolved leaving the composite structure shown in Figure 4b. With the increase of the NT film's thickness, the diffusion of F^- became slow, resulting in the decrease of $v_{electro}$. So, the free-standing NTs rather than the nanoporous morphology were formed (Figure 4c). Subsequently, the bundling TiO_2 films formed with increasing pore size and length, and the bundling layer and the debris can be easily removed by ultrasonication (Figure 4d−g). From these results we can see that the competitive reaction of v_{dis} and $v_{electro}$ played different role at different stage. By controlling the reaction time we can also adjust the morphologies, the sizes, and the lengths of TiO_2 NTs.

3.5. Effect of Applied Voltages. Figure 5 shows the FESEM images of samples prepared in the 0.5 wt % NH_4F and 2 vol % HF ethylene glycol electrolyte solution anodized at 20 °C for 1 h with various anodization voltage from 10

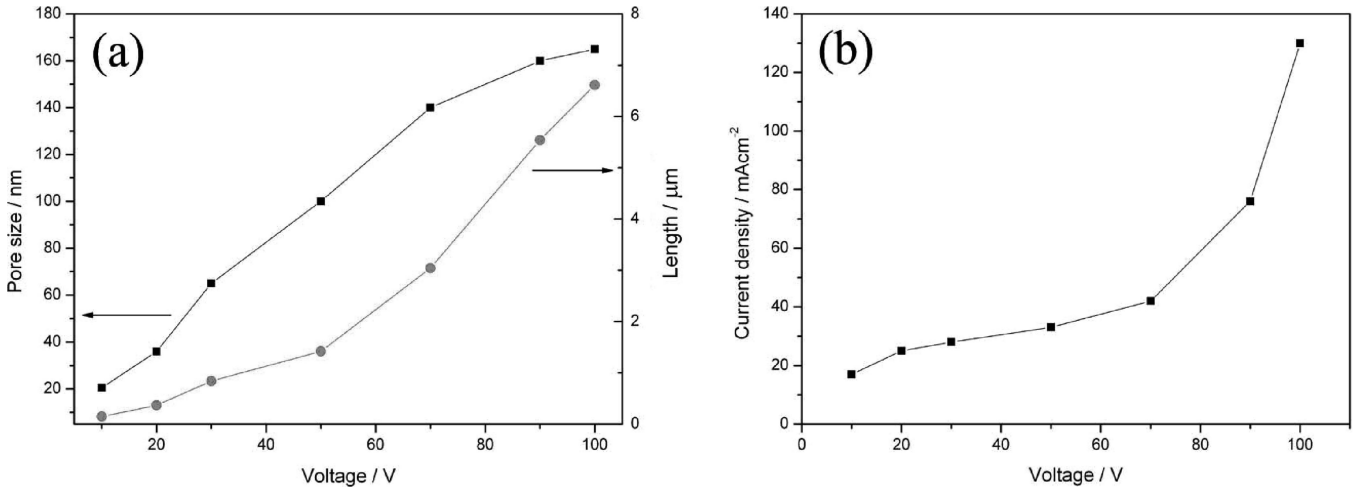

Figure 8. (a) Variation of TiO_2 nanotube length and pore size as functions of anodization voltage at 20 °C for 1 h. (b) Stable current density with different anodization voltage from 10 to 100 V.

(a) to 100 V (g), respectively. From these images it is seen that the TiO_2 NTs can be formed at all anodization voltages from 10 to 100 V. At low anodization voltages (10 V and 20 V), the electrochemical anodization speed was very slow and the NTs had very small pore sizes and length in the ranges of 21 and 40 nm and 380 and 600 nm, respectively. However, the v_{dis} was larger than $v_{electro}$ so that no nanoporous layer was formed on the top of NTs. Upon further increase the anodization voltage up to 70 V, the $v_{electro}$ increased as indicated from with the increase of the NT length and the pore size, while the v_{dis} was still larger than the $v_{electro}$. When further increasing the anodization voltage, the $v_{electro}$ exceeded the v_{dis}. The nanoporous TiO_2 NTs were consequently formed (Figure 5f,g), and decrease of pore size was observed (Figure 6a).

As a comparative test, Figure 7 shows the FESEM images of samples prepared under the same conditions except for that in 4 vol % HF electrolyte. As discussed above, the increase in the concentration of HF leads to faster chemical etching reaction. Free-standing NTs will be more favorably generated. It is seen from comparison between Figure 7 and Figure 5 that from 10 V to 100 V, no transition from free-standing morphology to nanoporous morphology was observed. The length of the NTs formed in 4 vol % HF was smaller than that formed in 2 vol % HF, and the pore size formed in 4 vol % HF was larger than that formed in 2 vol % HF. The relationships among anodization voltage, pore size, and length of the NTs are shown in Figure 8a, and the relationship between the anodization voltage and the current density is shown in Figure 8b. Different from the results shown in Figure 6a, the pore size increased monotonically at all the anodic voltage since the TiO_2 deposition speed was always lower than the chemical etching speed.

From the above results, it is seen that the competitive reactions of the electrochemical anodization and the chemical etching determine the growth speed and the morphology of TiO_2 NT arrays. The temperature, electrolyte's concentration, and reactive voltage together affect the balance between the two reactions and thus the final morphologies, diameters, and length by changing these reaction conditions simply. Also, we can predict the morphology evolution by changing one of them, which is of importance toward the production of desired nanostructures. From Figures 7 and 8, it is seen that anodization at high HF concentration cannot achieve high aspect ratio NTs and nanoporous NTs. Then one can think about (1) decreasing the HF concentration, (2) lowering the temperature, and (3) increasing the anodization speed. Figure 9 shows the results after changing the anodization conditions by increasing the anodization voltages and decreasing the HF concentration to 0.5% and the temperature to 0°. It is clearly seen that the nanopores became very clear and very regular at this time, and the pore size can be well controlled from 72 to 120 nm. Most attractively, the TiO_2 NT arrays can be prepared very rapidly from 23 to 61 μm for 1 h when increasing the voltages from 120 V to 200 V. The anodization at high voltages represents a new development toward fast achievement of TiO_2 NTs. Moreover, the nanoporous morphology can further evolve to the free-standing TiO_2 NT arrays by adding a bit more H^+ or at a higher temperature for a certain time (mostly a short time). (The data are not shown.)

3.6. Photoelectrochemical and Photocatalytic Properties. Shown in Figure 10 is the photoelectrochemical response of the selected TiO_2 NT samples under the monochromatic excitation from 250 nm to 600 nm and the applied bias of 0.5 V (vs SCE). The current density was collected by the electrochemical workstation with a three-electrode system including a Pt counter electrode and the crystal anatase TiO_2 NTs as the working electrode. All the samples have the similar pore size of about 120 nm. From the results we can see that all the TiO_2 NTs had obvious photocurrent response between 280 nm and 390 nm, and the maximum photocurrent response appeared at 355 nm. The porous TiO_2 NTs arrays had the higher photocurrent density than the free-standing NTs without top porous structure despite that they had less contact area. The reason is supposed to be due to bundling induced defects and so recombination. The TiO_2 arrays with the longer NTs had higher photocurrent density than the shorter NT array because they can absorb more energy of the UV illumination and collect more electrons to pass

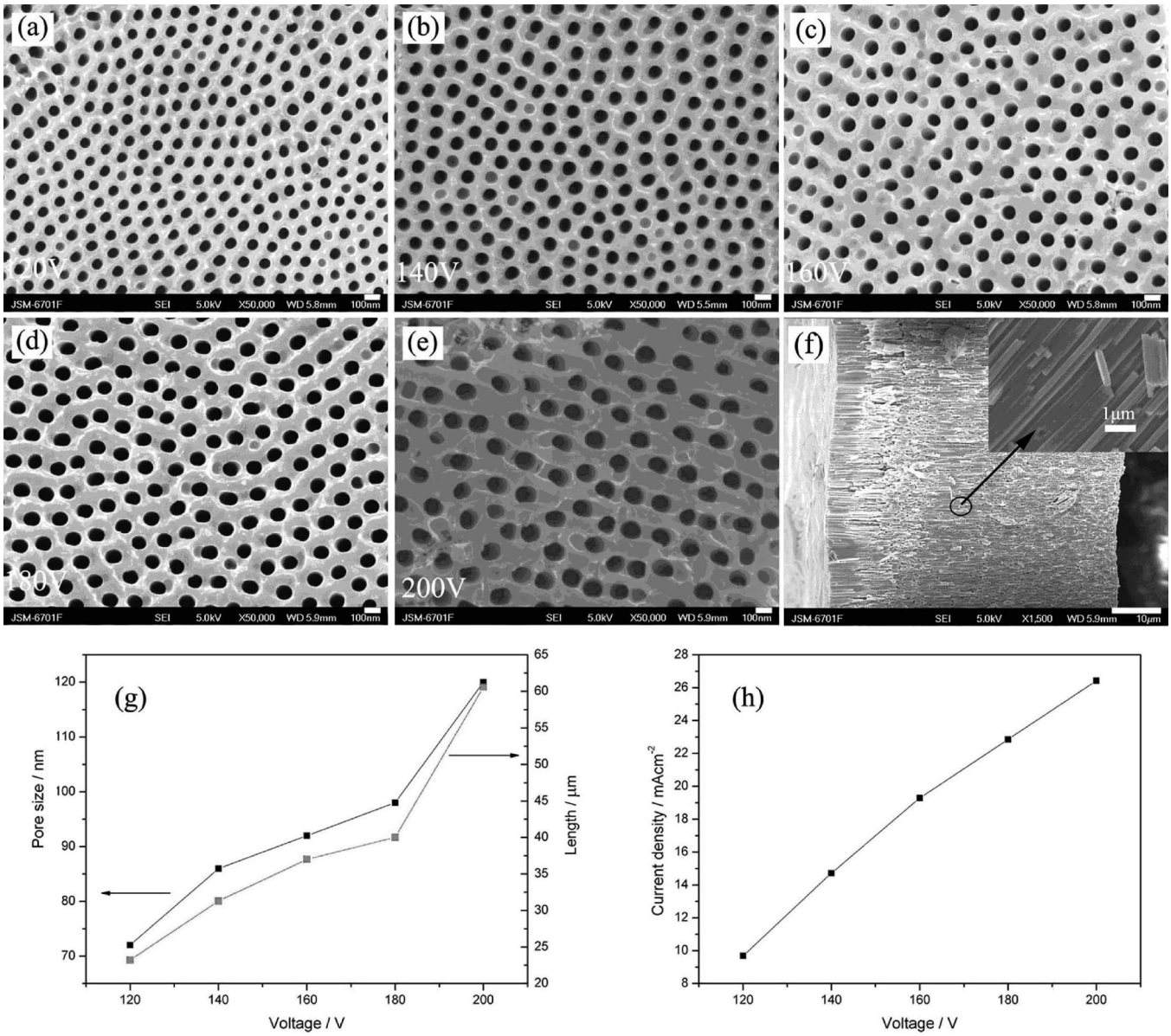

Figure 9. FESEM images of TiO_2 NTs array grown from a 0.5 wt % NH_4F and 0.5 vol % HF ethylene glycol electrolyte for 1 h at 0 °C with various anodization voltages from 120 (a) to 200 V (e), respectively. Cross sectional image of (e) is seen in (f). (g) The evolution of pore size and the length of NTs with anodization voltage. (h) Stable current density with different anodization voltages from 10 to 100 V.

through. From these results it is seen that the TiO_2 NTs with the porous top surface structure have a more significant advantage for charge transport than that without porous structure. The bundling and microcrack structure in free-standing TiO_2 NTs can deteriorate electron transport and enhance the recombination. Although the post-treatment of TiO_2 NTs in the supercritical CO_2 can significantly improve the alignment of conventional NTs, the defects are still many[19] and far from being resolved. The present work provides a direct approach to perfect alignment of NTs, bringing about reasonably enhanced electron transport efficiency, and is expected to find widespread applications in relevant areas.

Photocatalytic activity of the TiO_2 NTs was evaluated by phtocatalytic degradation of methylene blue in water at neutral pH. Shown in Figure 11 is the observed degradation of methylene blue vs illumination time catalyzed with different samples. The inset is the adsorption spectrum of the methylene blue solution at different photodegradation periods. The photocatalytic degradation of methylene blue, however, showed a different scenario; the NT arrays without top porous structure have better performance than the porous NTs. This is ascribed to the larger contact area between NTs and solutions as evaluated from the SEM images. The NT arrays with longer NTs have better photocatalytic activity which is not consistent with the report of the degradation of phenol.[23]

4. Conclusion

In summary, we have demonstrated how the balance between the electrochemical anodization and chemical etching can be utilized to control the surface morphology in anodization synthesis of TiO_2 NTs array. By changing the reaction temperature, the applied voltage, and the concentration of HF, the either nanoporous TiO_2 NTs or the free-

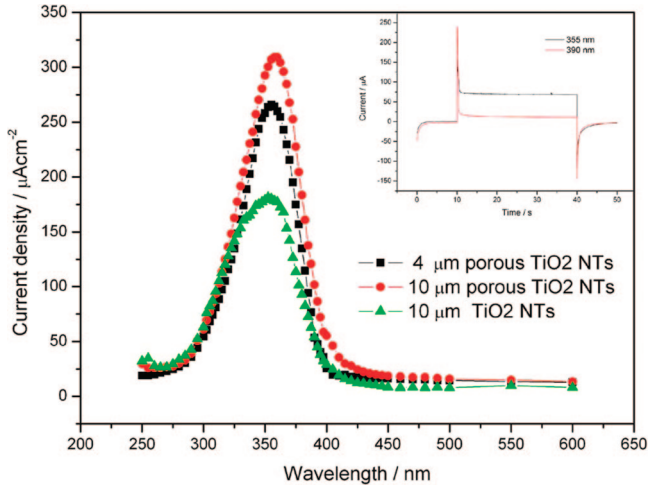

Figure 10. Variation of photocurrent density as a function of different illuminations from 250 nm to 600 nm in methylene blue solution for the prepared TiO_2 NTs arrays. The inset is the current−time curves of the 4 μm porous TiO_2 NTs under the illumination of 355 nm and 390 nm.

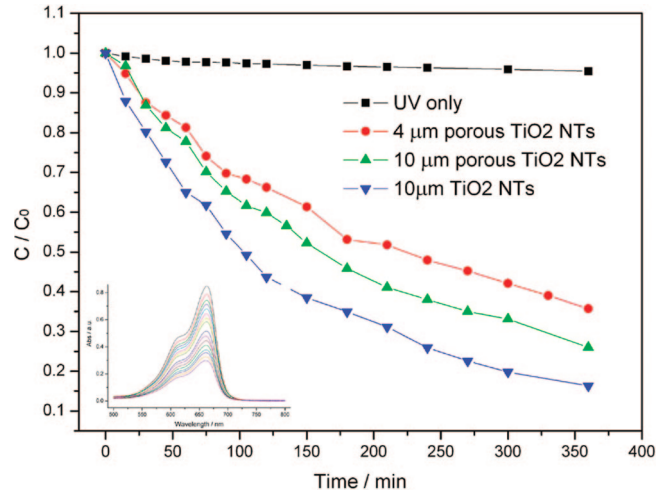

Figure 11. Comparison of the photocatalytic decomposition of methylene blue after 355 nm laser excitation, monitored at 664 nm, of catalyzed by UV only, porous or nonporous TiO_2 NTs arrays with different lengths. The inset shows the absorption spectrum of methylene blue with different reaction times.

standing NTs were obtained with tunable pore size, length, and wall thickness. Electrochemical etching (applied voltage) and low temperature are helpful for the formation of nanoporous morphology and high temperature and high HF concentration help to achieve the free-standing NT morphology. The photoelectrochemical response and the photocatalytic properties show different scenarios: the free-standing NTs have better photocatalytic property as a result of the larger surface area, and photoelectrochemical response is more dependent on the alignment of NTs, which makes nanoporous NTs have better response.

Acknowledgment. The authors gratefully acknowledge the "Hundred Talents Program" of Chinese Academy of Sciences and the NSFC (50721062, 50835009).

CM802384Y

(23) Liu, Z.; Zhang, X.; Nishimoto, S.; Jin, M.; Tryk, D. A.; Murakami, T.; Fujishima, A. *J. Phys. Chem. C* **2008**, *112*, 253.